ARMY RESEARCH LABORATORY

A Geometrically Nonlinear Phase Field Theory of Brittle Fracture

by JD Clayton and J Knap

ARL-RP-0511 October 2014

A reprint from the Int J Fract, 2014;189(2):139–148.
Published online in the Springer Science+Business Media Dordrecht [accessed 2014 Aug 19].
http://link.springer.com/article/10.1007/s10704-014-9965-1.

NOTICES

Disclaimers

The findings in this report are not to be construed as an official Department of the Army position unless so designated by other authorized documents.

Citation of manufacturer's or trade names does not constitute an official endorsement or approval of the use thereof.

Destroy this report when it is no longer needed. Do not return it to the originator.

Army Research Laboratory
Aberdeen Proving Ground, MD 21005-5069

ARL-RP-0511 **October 2014**

A Geometrically Nonlinear Phase Field Theory of Brittle Fracture

JD Clayton and J Knap
Weapons and Materials Research Directorate, ARL

A reprint from the Int J Fract, 2014;189(2):139–148.
Published online in the Springer Science+Business Media Dordrecht [accessed 2014 Aug 19].
http://link.springer.com/article/10.1007/s10704-014-9965-1.

REPORT DOCUMENTATION PAGE

Form Approved
OMB No. 0704-0188

1. REPORT DATE *(DD-MM-YYYY)*	2. REPORT TYPE	3. DATES COVERED (From - To)
October 2014	Reprint	October 2013–October 2014

4. TITLE AND SUBTITLE
A Geometrically Nonlinear Phase Field Theory of Brittle Fracture

5a. CONTRACT NUMBER

5b. GRANT NUMBER

5c. PROGRAM ELEMENT NUMBER

6. AUTHOR(S)
JD Clayton and J Knap

5d. PROJECT NUMBER

5e. TASK NUMBER

5f. WORK UNIT NUMBER

7. PERFORMING ORGANIZATION NAME(S) AND ADDRESS(ES)
US Army Research Laboratory
ATTN: RDRL-WMP-C
Aberdeen Proving Ground, MD 21005-5069

8. PERFORMING ORGANIZATION REPORT NUMBER
ARL-RP-0511

9. SPONSORING/MONITORING AGENCY NAME(S) AND ADDRESS(ES)

10. SPONSOR/MONITOR'S ACRONYM(S)

11. SPONSOR/MONITOR'S REPORT NUMBER(S)

12. DISTRIBUTION/AVAILABILITY STATEMENT
Approved for public release; distribution is unlimited.

13. SUPPLEMENTARY NOTES
A reprint from the Int J Fract, 2014;189(2):139–148. Published online in the Springer Science+Business Media Dordrecht [accessed 2014 Aug 19]. http://link.springer.com/article/10.1007/s10704-014-9965-1.

14. ABSTRACT
Phase field theory is developed for solids undergoing potentially large deformation and fracture. The elastic potential depends on a finite measure of elastic strain. Surface energy associated with fracture can be anisotropic, enabling description of preferred cleavage planes in single crystals, or isotropic, applicable to amorphous solids such as glass. Incremental solution of the Euler–Lagrange equations corresponds to local minimization of an energy functional for the solid, enabling prediction of equilibrium crack morphologies. Predictions are in close agreement with analytical solutions for pure mode I or pure mode II loading, including the driving force for a crack to extend from a pre-existing plane onto a misoriented cleavage plane. In an isotropic matrix, the tendency for a crack to penetrate or deflect around an inclusion is shown to depend moderately on the ratio of elastic stiffness in matrix and inclusion and strongly on their ratio of surface energy. Cracks are attracted to (shielded by) inclusions softer (stiffer) than the surrounding matrix. The theory and results apparently report the first fully three-dimensional implementation of phase field theory of fracture accounting for simultaneous geometric nonlinearity, nonlinear elasticity, and surface energy anisotropy.

15. SUBJECT TERMS
brittle fracture, phase field, nonlinear elasticity, elastic inclusion, ceramics

16. SECURITY CLASSIFICATION OF:			17. LIMITATION OF ABSTRACT	18. NUMBER OF PAGES	19a. NAME OF RESPONSIBLE PERSON
a. REPORT	b. ABSTRACT	c. THIS PAGE			JD Clayton
Unclassified	Unclassified	Unclassified	UU	16	19b. TELEPHONE NUMBER (*Include area code*) 410-278-6146

Int J Fract (2014) 189:139–148
DOI 10.1007/s10704-014-9965-1

ORIGINAL PAPER

A geometrically nonlinear phase field theory of brittle fracture

J. D. Clayton · J. Knap

Received: 8 May 2014 / Accepted: 29 July 2014 / Published online: 19 August 2014

Abstract Phase field theory is developed for solids undergoing potentially large deformation and fracture. The elastic potential depends on a finite measure of elastic strain. Surface energy associated with fracture can be anisotropic, enabling description of preferred cleavage planes in single crystals, or isotropic, applicable to amorphous solids such as glass. Incremental solution of the Euler–Lagrange equations corresponds to local minimization of an energy functional for the solid, enabling prediction of equilibrium crack morphologies. Predictions are in close agreement with analytical solutions for pure mode I or pure mode II loading, including the driving force for a crack to extend from a pre-existing plane onto a misoriented cleavage plane. In an isotropic matrix, the tendency for a crack to penetrate or deflect around an inclusion is shown to depend moderately on the ratio of elastic stiffness in matrix and inclusion and strongly on their ratio of surface energy. Cracks are attracted to (shielded by) inclusions softer (stiffer) than the surrounding matrix. The theory and results apparently report the first fully three-dimensional implementation of phase field theory of fracture accounting for simultaneous geometric nonlinearity, nonlinear elasticity, and surface energy anisotropy.

Keywords Brittle fracture · Phase field · Nonlinear elasticity · Elastic inclusion

J. D. Clayton (✉)
Impact Physics, US ARL,
Aberdeen, MD 21005-5066, USA
e-mail: jclayton@arl.army.mil

J. Knap
Computational Science, US ARL,
Aberdeen, MD 21005-5066, USA

1 Introduction

Brittle solids—which include ceramics, typical rocks and minerals, glass, and some metals—demonstrate a tendency to fracture rather than deform plastically (e.g., by dislocation glide) when subjected to stresses exceeding their elastic limit. Brittle solids often demonstrate strong directional bonding at the atomic scale and a relatively large ratio of shear to bulk modulus (Gilman 2003), though exceptions are possible. In crystalline solids, fractures may be transgranular (i.e., cleavage Lawn 1968; Schultz et al. 1994) or intergranular (i.e., at grain boundaries), while in amorphous or glassy solids, fractures are independent of intrinsic microstructure but highly dependent on pre-existing flaws, especially surface flaws (Wilshaw 1971). In ceramics and glass, depending on loading conditions, fractures may consist of dominant crack(s) or distributed micro-cracks (Lawn et al. 1994). Performance of ceramics in structural applications is most often inhibited by their low fracture toughness. Toughness can often be improved by modifying the microstructure to promote crack bridging (i.e., deflection or pull-out at second-phase particles, grain boundaries, or other heterogeneities), thus

shielding stresses experienced by a propagating crack and causing it to meander or arrest. Efforts to improve ductility of ceramics and ceramic nanocomposites in this manner include controlled introduction of weak interfaces, coarsening and elongating the grain structure, and embedding the polycrystal with strong inclusions (Faber and Evans 1983; Lawn et al. 1994; Ohji et al. 1998).

Resistance to fracture is often the controlling factor limiting applications in which a brittle material can be used; grain size and morphology can be engineered to optimize effective ductility, impact resistance, or fatigue life for a given application (Lawn et al. 1994; Wiederhorn 1984). Selection or design of a material for such an application requires understanding afforded by a predictive model of fracture. Computer simulations enable descriptions of fracture in brittle solids under complex loading conditions and for nonlinear and anisotropic material behaviors, difficult, if not impossible, to address using existing analytical methods (e.g., solutions available from linear elastic fracture mechanics). Engineering finite element (FE) simulations often invoke continuum damage mechanics theories, wherein the tangent stiffness of a material element degrades as "damage" accumulates. Conventional continuum damage mechanics theories (Clayton and McDowell 2003, 2004; Sun and Khaleel 2004; Clayton 2006, 2008) require prescription of phenomenological kinetic equations specifying the rate of damage accumulation; associated parameters in such equations must be tuned to experiments similar to those simulated numerically. Furthermore, solutions can depend on mesh size. Simple models based on the notion of theoretical strength (Gilman 1960; Clayton 2009, 2010) can provide insight into directionality of fracture resistance but do not enable prediction of morphological crack evolution for complex stress states. Cohesive models of fracture (Xu and Needleman 1993; Espinosa and Zavattieri 2003; Clayton 2005; Arias et al. 2007; Foulk and Vogler 2010) enable simulation of discrete cracks and branching; however, mesh construction should not be arbitrary since crack paths are constrained to follow element boundaries. Extended FE methods (Moes et al. 1999) alleviate the latter problem by permitting discontinuities to traverse elements, but predictive physics is compromised since the crack propagation direction must be specified by a user-defined criterion. Similarly, numerical methods involving incremental crack growth laws (Kim et al. 1996) require specification of criteria for crack extension such as maximum energy release (Nuismer 1975). Multi-scale techniques (Knap and Ortiz 2003; Zhang et al. 2007) blending atomic and continuum theory appear promising for describing problems wherein localized damage or defects are contained within a relatively small volume of the entire body, but are inhibited by difficulties with linking discrete and continuous regions and attendant numerical complexity; purely atomic methods (Knap and Sieradzki 1999) are necessarily restricted to relatively small system sizes and to short time scales for dynamic simulations.

Phase field theories of fracture (Jin et al. 2001; Eastgate et al. 2002; Del Piero et al. 2007; Hakim and Karma 2009; Kuhn and Muller 2010; Abdollahi and Arias 2012; Alber 2012; Borden et al. 2012; Hofacker and Miehe 2012; Spatschek et al. 2011; Voyiadjis and Mozaffari 2013) enable prediction of complex fracture processes without introduction of spurious physics. Apart from the usual elastic constants, essential material parameters entering such theories can usually be directly related to surface energy and diffuse interfacial width, the latter associated with regularization inherent in the phase field approach that renders solutions mesh size independent. In essence, fractures evolve naturally with applied loading as the body seeks minimum energy configurations. Mathematical analysis (Del Piero et al. 2007) has demonstrated aspects of Γ-type convergence of certain variational models towards sharp interface models of Griffith type as interfacial width is reduced.

This paper develops a phase field theory for fracture of nonlinear elastic materials based on a variational approach, with numerical implementation involving incremental minimization of a suitable free energy functional. The present novel model, whose governing (Euler–Lagrange) equations are derived in an analogous way to an existing theory for deformation twinning (Clayton and Knap 2011a), is similar to a finite strain variational model implemented in two dimensions (Del Piero et al. 2007), but is new in its incorporation of anisotropy and fully three-dimensional (3D) FE implementation. Previous phase field approaches have considered anisotropic fracture energy (Jin et al. 2001; Hakim and Karma 2009), albeit in the context of linear elasticity and 2D numerical simulations. Furthermore, these and most other prior works (Eastgate et al. 2002; Kuhn and Muller 2010; Abdollahi and Arias 2012; Alber 2012; Borden et al. 2012; Hofacker and

Miehe 2012; Voyiadjis and Mozaffari 2013) invoked a dynamic approach, requiring specification of one or more parameters controlling the time scale of fracture kinetics. In contrast, the present model invokes incremental energy minimization, enabling the solution of quasi-static fracture problems without the need for kinetic parameter(s). This work represents the first fully 3D implementation of a phase field theory of fracture accounting for geometric nonlinearity, nonlinear elasticity, and possible surface energy anisotropy. Results of numerical simulations of mode I and mode II loading validate the model. Simulation results on crack deflection around or penetration through a spherical inclusion then follow, providing new insight into crack–inclusion interactions in nonlinear elastic solids not available from 2D linear analytical solutions (Tamate 1968; Atkinson 1972; Erdogan et al. 1974; Evans 1974).

2 Phase field theory

2.1 Governing equations

Finite deformation theory (Clayton 2011; Clayton and Knap 2011a,b, 2013) is used, where $\boldsymbol{x} = \boldsymbol{x}(\boldsymbol{X}) = \boldsymbol{X} + \boldsymbol{u}(\boldsymbol{X})$ are spatial Cartesian coordinates of a material particle initially at $\boldsymbol{X}$. Let ∇ denote the material gradient operator. The deformation gradient, symmetric finite deformation tensor, and ratio of deformed to initial volume are, respectively,

$$\boldsymbol{F} = \nabla \boldsymbol{x} = \mathbf{1} + \nabla \boldsymbol{u}, \quad \boldsymbol{C} = \boldsymbol{F}^{\mathrm{T}}\boldsymbol{F}, \quad J = \sqrt{\det \boldsymbol{C}}. \tag{1}$$

Degrees of freedom are displacement $u(X)$ and order parameter $\eta(X)$, where $\eta = 0$ for perfect material, $\eta = 1$ for fully fractured material, and $\eta \in (0, 1)$ within diffuse interfaces between intact and failed domains, for example. The total free energy functional for the body Ω is

$$\Psi(\boldsymbol{u}, \eta) = \int_{\Omega} [W(\nabla \boldsymbol{u}, \eta) + \frac{\Gamma}{l}\eta^2 + \boldsymbol{\kappa} : \nabla\eta \otimes \nabla\eta] \mathrm{d}\Omega. \tag{2}$$

Elastic strain energy per unit reference volume is W and may degrade with increasing η, surface energy per unit reference area is Γ, constant l is proportional to the equilibrium crack width or thickness of the diffuse interface, and $\boldsymbol{\kappa}$ is a symmetric second-order material property tensor, in what follows of the form

$$\boldsymbol{\kappa} = \Gamma l[\mathbf{1} + \beta(\mathbf{1} - \mathbf{m} \otimes \mathbf{m})], \tag{3}$$

with $\boldsymbol{m}$ a unit normal vector to a preferred cleavage plane in a crystal, for example. Parameter β penalizes fractures on planes with orientations different than $\boldsymbol{m}$. For isotropic surface energy, e.g., as in a glass or a representation of a macroscopically homogeneous brittle isotropic solid, $\beta = 0$. From functional (2), respective Euler–Lagrange equations in Ω and boundary conditions on its external surface $\partial\Omega$ are derived using standard variational methods and the divergence theorem (Clayton and Knap 2011a):

$$\nabla \cdot \boldsymbol{P} = 0, \quad \partial W/\partial \eta + 2\Gamma\eta/l = 2\nabla \cdot \boldsymbol{\kappa}\nabla\eta; \tag{4}$$

$$\boldsymbol{t} = P\boldsymbol{n}, \quad h = 2\boldsymbol{\kappa} : \nabla\eta \otimes \boldsymbol{n}. \tag{5}$$

First Piola–Kirchhoff stress is $\boldsymbol{P} = \partial W/\partial \boldsymbol{F} = \partial W/\partial \nabla \boldsymbol{u}$ and is generally not symmetric, traction on a surface element with reference normal $\boldsymbol{n}$ is $\boldsymbol{t}$, and h is a conjugate force to η on boundary $\partial\Omega$ (note that $h = 0$ along a free surface).

2.2 Elasticity

Similarly to previous phase field models for twinning (Clayton and Knap 2011b, 2013), compressible neo-Hookean elasticity is considered with the following strain energy density function:

$$W(\boldsymbol{C}, \eta) = \frac{1}{2}[\lambda(\ln J)^2 - \mu(2\ln J - \mathrm{tr}\boldsymbol{C} + 3)]. \tag{6}$$

Lamé coefficients μ and λ depend on order parameter η and possibly volume change measure J:

$$\mu(\eta) = \mu_0[\zeta + (1-\zeta)(1-\eta)^2], \quad \lambda(\eta, J) = k - \frac{2}{3}\mu. \tag{7}$$

Shear modulus μ degrades from its reference value μ_0 to a minimum value $\zeta\mu_0$ in fully fractured domains, where $0 < \zeta \ll 1$. Bulk modulus k degrades in tension but not in compression, in order to prohibit interpenetration:

$$k = k_0\{[\zeta + (1-\zeta)(1-\eta)^2]\langle J - 1\rangle + \langle 1 - J\rangle^*\}. \tag{8}$$

The initial (not degraded) bulk modulus is $k_0 = \lambda_0 + \frac{2}{3}\mu_0$. The following notation applies: $\langle x\rangle = 1 \forall x > 0$, $\langle x\rangle = 0 \forall x \leq 0$, $\langle x\rangle^* = 1 \forall x \geq 0$, and $\langle x\rangle^* = 0 \forall x < 0$. Poisson's ratio in the undamaged solid is $\nu = \lambda_0/(2\lambda_0 + 2\mu_0)$. The stress tensor is then, invoking (6),

$$\boldsymbol{P} = \mu \boldsymbol{F} + (\lambda \ln J - \mu)\boldsymbol{F}^{-\mathrm{T}} + \frac{1}{2} J (\ln J)^2 (\partial k / \partial J) \boldsymbol{F}^{-\mathrm{T}}. \quad (9)$$

The rightmost term accounts for tension-compression asymmetry in the degradation of the bulk stiffness. Anisotropic elastic constants are not included here but may be considered in the future by adapting methods in Clayton and Knap (2011a); however, in many single crystals, surface energy anisotropy is thought to dominate elastic anisotropy (Lawn 1968).

For purposes of comparison with known analytical solutions, linear elasticity is also sometimes considered in this work, whereby the strain energy density function is

$$W(\nabla \boldsymbol{u}, \eta) = \frac{1}{2}\lambda(\nabla \cdot \boldsymbol{u})^2 + \frac{1}{4}\mu \mathrm{tr}\{[(\nabla \boldsymbol{u} + (\nabla \boldsymbol{u})^{\mathrm{T}})]^2\}, \quad (10)$$

and elastic coefficients degrade in the same way as in (7) and (8), with volume change in the linear approximation $J \rightarrow 1 + \nabla \cdot \boldsymbol{u}$. The stress tensor [derivative of (10) with respect to $\nabla \boldsymbol{u}$] in the linear theory is symmetric:

$$\boldsymbol{P} = \lambda(\nabla \cdot \boldsymbol{u})\boldsymbol{1} + 2\mu(\nabla \boldsymbol{u})_{\mathrm{sym}} + \frac{1}{2}(\nabla \cdot \boldsymbol{u})^2 (\partial k / \partial \nabla \boldsymbol{u})\boldsymbol{1}. \quad (11)$$

Comparison of nonlinear and linear results also enables evaluation of possible importance of nonlinear aspects of the model and thereby may suggest domains of valid loading regimes for the linear theory.

The present model permits degradation of the bulk modulus only when volume change is tensile and degradation of the shear modulus regardless of whether loading is tensile or compressive. This approach, which is analogous to that implemented in Amor et al. (2009) and one described in Spatschek et al. (2011), enables the material to lose shear strength even when all three principal strain components are negative. A different theory implemented in Miehe et al. (2010), Hofacker and Miehe (2012), Borden et al. (2012) in the small strain setting decomposes the strain tensor into positive and negative parts following diagonalization. The elastic strain energy dependent on the positive (tensile) components degrades upon fracture, while the compressive energy is unaffected by damage (i.e., does not vary with changing values of the order parameter). In contrast to the present approach, shear strength loss does not occur when all three principal strains are compressive (Borden et al. 2012). Suitability of one approach over the other likely depends on the material and loading regime, and could be evaluated by considering the failure behavior of a material subjected to triaxial compression (Murrell 1965) or shock compression under lateral pre-stress (Clayton 2014). In brittle solids such as ceramics and rocks, when confining or lateral stress is not too large, shear fractures may occur under compression, but extreme lateral stress/pressure may suppress propagation of mode II cracks due to frictional resistance that tends to increase with increasing confinement (Murrell 1965; Clayton 2010).

3 Numerical implementation

The theory is implemented numerically using Lagrangian finite elements, following general procedures outlined in Clayton and Knap (2011a). Incremental solutions to (4) are sought using conjugate gradient minimization of total energy functional Ψ of (2), subject to constraints associated with external boundary conditions on $\partial\Omega$. Let $\delta\eta(\boldsymbol{X})$ be a local change in order parameter η at material point $\boldsymbol{X}$ induced by incremental loads. The additional internal constraint $\delta\eta(\boldsymbol{X}) \geq 0$ if $\eta(\boldsymbol{X}) \geq 0.9$ is used to render fracture irreversible (Del Piero et al. 2007).

In the current implementation of the phase field theory, cracks represented by positive values of the order parameter are predicted to follow paths dictated by incremental total energy minimization, subject to the irreversibility constraint described above. When this constraint is active, the incremental energy minimization problem can be viewed as minimization of energy of an alternative system with time dependent boundary conditions associated with introduction of new surfaces along which $\eta \geq 0.9$ is prescribed; equilibrium equations (4) remain satisfied in solutions thus obtained for this alternative system. If the irreversibility constraint on $\delta\eta$ is not enforced, then damage is reversible and cracks will heal fully upon unloading, a feature noted in other phase field models (Hakim and Karma 2009). If damage is regarded as completely irreversible, then dissipated energy can be defined as the contribution to Ψ of the final two terms in the integrand of (2) corresponding to the surface energy of fracture associated with the order parameter and its spatial gradient. This is consistent with definitions of dissipated energy used elsewhere (Miehe et al. 2010; Borden et al. 2012; Spatschek et al. 2011) when viscous effects are omit-

ted. Another definition of dissipated energy, valid for partial reversibility of damage, could be constructed for a loading–unloading cycle: net dissipated energy could be measured by the difference between work expended and then recovered by the boundary conditions, minus any residual energy remaining in the system upon external unloading. Further review of capabilities of phase field approaches to predict crack paths can be found in Spatschek et al. (2011).

In order to make the results broadly accessible and applicable to a number of classes of brittle materials, numerical analyses are performed later in the context of dimensionless parameters rather than property sets peculiar to any specific solid. Energy density can be normalized by μ_0, such that W/μ_0 depends only on ν and other terms in the integrand of (2) depend on dimensionless constants $\bar{\Gamma} = \Gamma/\mu_0 l$, β, and ζ. Taking $\zeta = 0.01$ and $l/R_0 =$ constant, where R_0 is a fixed characteristic length associated with the problem of interest, dimensionless solutions depend only the choice of $\{\nu, \bar{\Gamma}, \beta\}$, where $\beta = 0$ for isotropy. Properties representative of brittle solids are later chosen as $\nu = 0.25$ and $\bar{\Gamma} = 0.01$, while β and $\boldsymbol{m}$ are explored parametrically.

In order to evaluate accuracy and validity of the model, simulations on a block of elastic material with a pre-existing straight crack/notch are performed. The block is of reference dimensions $50R_0 \times 50R_0 \times 25R_0$, where $R_0 = 2l$ is the finite radius of the initial notch tip, and the initial crack/notch is of length $a = 25R_0$. The plane of this pre-crack is $X_2 = 0$ in local Cartesian reference coordinates, and let (r, θ) be local reference polar coordinates with origin at the notch tip. Along the outer boundary, displacement boundary conditions are imposed for either pure mode I or pure mode II loading (Zhang et al. 2007; Rice 1968); e.g., for mode I:

$$u_1 = \Delta\sqrt{\frac{4ar}{2\pi}}\cos\frac{\theta}{2}\left(1 - 2\nu + \sin^2\frac{\theta}{2}\right), \tag{12}$$

$$u_2 = \Delta\sqrt{\frac{4ar}{2\pi}}\sin\frac{\theta}{2}\left(2 - 2\nu - \cos^2\frac{\theta}{2}\right), \tag{13}$$

where the load parameter is $\Delta = K_\mathrm{I}/2\mu\sqrt{a}$. Similar equations apply for mode II, where $\Delta = K_\mathrm{II}/2\mu\sqrt{a}$ (Clayton and Knap 2013). For a sharp crack in an infinite medium, linear elastic fracture mechanics predicts crack extension will occur when $\Delta \geq K_\mathrm{C}/2\mu\sqrt{a}$, where $K_\mathrm{C} = \sqrt{2\mu G/(1-\nu)}$, and $G = 2\Gamma$ for an isotropic material. Because of the finite domain and crack radius, values of $K_{\mathrm{I/II}}$ entering Δ are corrected herein by computing the $\mathfrak{J}$-integral (Rice 1968) numerically. Linear elastic fracture concepts (e.g., $\mathfrak{J} = G$) are used only to define boundary conditions and aid in analysis and interpretation of results; the phase field simulations do not directly incorporate linear elastic fracture mechanics. To mimic plane strain $u_3 = 0$ is imposed along the boundary, and $h = 0$ is imposed on all external surfaces. Finite element meshes consist of $\approx$ 4M tetrahedral elements of size small relative to l to resolve order parameter gradients at fracture surfaces.

4 Numerical results

4.1 Cracking for isotropic and anisotropic surface energies

Propagation of a pure mode I crack in a notched body with isotropic surface energy ($\beta = 0$) is shown in Fig. 1a, b for nonlinear elasticity for two different load increments, and in Fig. 1c for linear elasticity. Initiation at the notch tip occurs at $K_\mathrm{I}/K_\mathrm{C} \simeq 1.03$ for both nonlinear and linear elasticity, validating the model for isotropic surface energy, and neo-Hookean elasticity predicts a 10–15 % longer crack than linear elasticity at the larger applied displacement. Figure 1d shows the effect of anisotropic surface energy with $\beta = 100$ for a cleavage plane twisted at angle $\phi = \pi/4$ relative to the pre-existing crack plane; i.e., $\boldsymbol{m} = [\cos\phi, 0, \sin\phi]$, where normalization of the loading for twist is (Wiederhorn 1984)

$$K_\mathrm{C} = \sqrt{2\mu G/(1-\nu)}\sec^2\phi \qquad \text{(twist)}. \tag{14}$$

Figure 1e shows a similar result for a cleavage plane tilted at angle $\phi = \pi/4$, i.e., $\boldsymbol{m} = [\cos\phi, \sin\phi, 0]$, where normalization for pure tilt misorientation is by the factor (Wiederhorn 1984; Xu et al. 2003)

$$K_\mathrm{C} = \sqrt{2\mu G/(1-\nu)}\sec^2(\phi/2) \qquad \text{(tilt)}. \tag{15}$$

Shown in Fig. 2a, b are components of first Piola–Kirchhoff stress tensor $\boldsymbol{P}$ of (9), normalized by the initial shear modulus. Stress concentrations are of large magnitude (e.g., locally on the order of 10 % of the modulus) but remain bounded in part due to the finite radius of the crack tip resolved numerically.

As validated in Fig. 3, the phase field model correctly predicts that twist misorientation resists crack

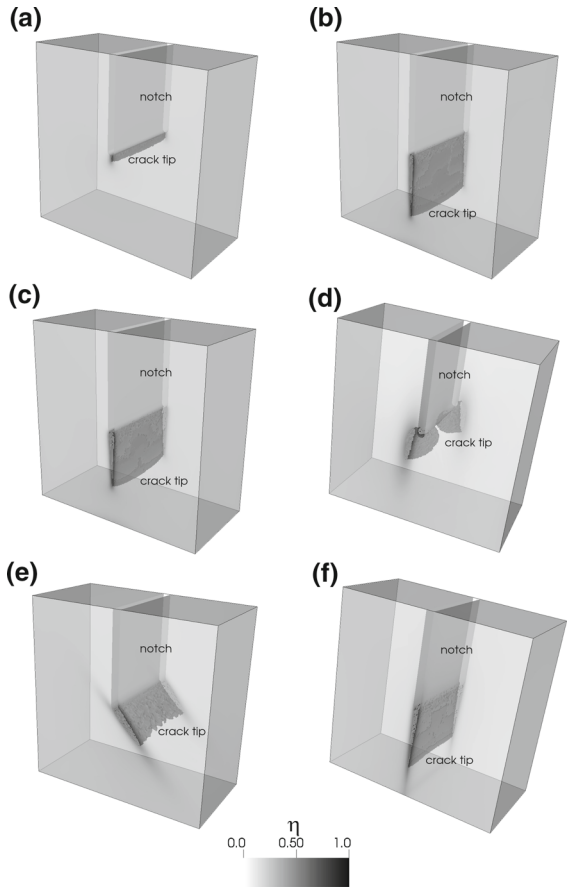

Fig. 1 Phase field predictions for pure mode I or mode II loading, with fractured material ($\eta > 0.7$) removed for visualization: **a** nonlinear elastic, $\beta = 0$, $K_I/K_C = 1.1$ **b** nonlinear elastic, $\beta = 0$, $K_I/K_C = 2.4$ **c** linear elastic, $\beta = 0$, $K_I/K_C = 2.4$ **d** nonlinear elastic, $\phi = \pi/4$ (twist), $\beta = 100$, $K_I/K_C = 1.1$ **e** nonlinear elastic, $\phi = \pi/4$ (tilt), $\beta = 100$, $K_I/K_C = 1.5$ (f) linear elastic, $\beta = 100$, $K_{II}/K_C = 1.5$

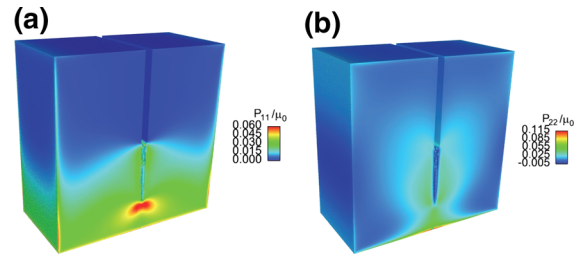

Fig. 2 Phase field predictions for pure mode I loading, nonlinear elastic, $\beta = 0$, $K_I/K_C = 2.4$, with fractured material ($\eta > 0.7$) removed for visualization: **a** normal stress component $P_{11}/\mu_0 = P_{xX}/\mu_0$ **b** normal stress component $P_{22}/\mu_0 = P_{yY}/\mu_0$ [referred here to global coordinates with (X, Y) oriented (normal, parallel) to the crack face]

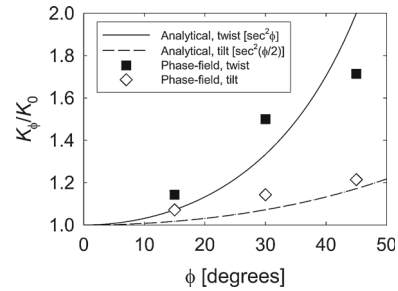

Fig. 3 Predictions of phase field model (nonlinear elastic, $\beta = 100$) for extension of a mode I crack on plane misoriented by an angle ϕ of twist or tilt from the original cleavage surface, compared to linear elastic fracture mechanics solution (Gell and Smith 1967; Wiederhorn 1984; Xu et al. 2003). K_ϕ/K_0 is the ratio of driving force for extension on the misoriented plane relative to that for $\phi = 0°$

propagation more than the same angle of tilt misorientation (Wiederhorn 1984). Figure 1f depicts a result for pure mode II loading with $\beta = 100$ set to favor crack propagation on $\boldsymbol{m} = [1, 0, 0]$. In all cases shown in Figs. 1 and 2, when imposed boundary displacements are large enough that cracks become overdriven (e.g., $K \gtrsim K_C$), they do not necessarily propagate completely through the specimen in an unstable manner because of the boundary conditions that tend to repel the crack as it approaches the lower edge and possible effects of nonzero ζ that serves to maintain some residual stiffness in the fully damaged material.

In the examples involving misorientation (Fig. 1d, e), cracks demonstrate non-uniform fronts suggestive of possible contributions of mode III loading. Presumably, such effects arise from the finite thickness of the domain in the X_3 direction, since far-field in-plane boundary conditions (12) and (13) apply for pure mode I loading of the initial notched configuration under plane strain. For the case shown in Fig 1d, dependence of the solution on X_3 is expected regardless since the cleavage plane normal $\boldsymbol{m}$ has a nonzero out-of-plane component, though the predicted cusps in the crack profile may be affected by or attributed to mode III-type contributions. Analytical solutions to which the simulation results are compared in Fig. 3, as stated in Wiederhorn (1984) and derived in Gell and Smith (1967), Xu et al. (2003) do not account for finite thickness effects. Their agreement with initiation predicted by the phase field simulations is reasonable, however, and it is noted that non-uniformity appears less pronounced at the onset of crack growth. The present

phase field theory, like the cited analytical solutions, prescribes a single fracture energy for a given material or interface, and does not distinguish among possibly different work of separation (toughness) values under modes I, II, and/or III. In contrast, some cohesive models of fracture such as those described in Espinosa and Zavattieri (2003) permit the freedom of different values of work of separation under different pure modes of loading as well as under mixed mode conditions.

4.2 Crack interaction with a spherical inclusion

A second set of phase field simulations considers the presence of an elastic inclusion embedded in an otherwise homogeneous matrix material of the same geometry (i.e., with notch or pre-crack of length $a = 50l$), and subjected to the same mode I displacement boundary conditions as considered in Figs. 1 and 2. The spherical inclusion has initial radius R_I, is centered at a distance $25l$ from the initial notch tip, and here obeys the same general constitutive laws as the matrix material, though inclusion and matrix may have different elastic stiffness and different dimensionless fracture energy $\bar{\Gamma}$. Both matrix and inclusion are assigned $\nu = 0.25$ (i.e., $\lambda_0 = \mu_0$) and $\beta = 0$ (isotropy). Depending on the mismatch in properties of the two materials, a propagating mode I crack will either penetrate the inclusion or deflect around it. Representative examples of the latter are shown in Fig. 4 (order parameter η) and Fig. 5 (normal and shear stress components for a planar slice of the three-dimensional domain). As demonstrated in Fig. 5, both normal and shear stresses are large but bounded near the crack tip as it propagates around the stiff and strong inclusion. Recall, on the other hand, that in linear elastic fracture mechanics, singularities arise at the crack tip (with shear stress vanishing at $\theta = 0$) for pure mode I loading (Rice 1968). The present phase field simulations, which omit anisotropy of fracture toughness and elastic constants, are physically representative of a brittle glassy material with perfect bonding between inclusion and matrix, for example.

Analytical solutions for crack–inclusion interactions (Tamate 1968; Atkinson 1972; Erdogan et al. 1974) idealize the problem as 2D and linear elastic, but do enable prediction of effects of elastic properties and geometry on local stress intensity factors. These works all predict a decrease in crack driving force as the stiffness of the inclusion increases. A similar effect is predicted by the phase field model, as shown in Fig. 6: for the same far-field boundary conditions, the crack moves closer to the soft inclusion than the stiff one. The present phase field approach predicts evolving crack geometry (i.e., growth) as the specimen deforms to possibly large local strains, whereas analytical results (Tamate 1968; Atkinson 1972; Erdogan et al. 1974) only indicate a tendency for crack extension from a pre-existing flaw of fixed geometry.

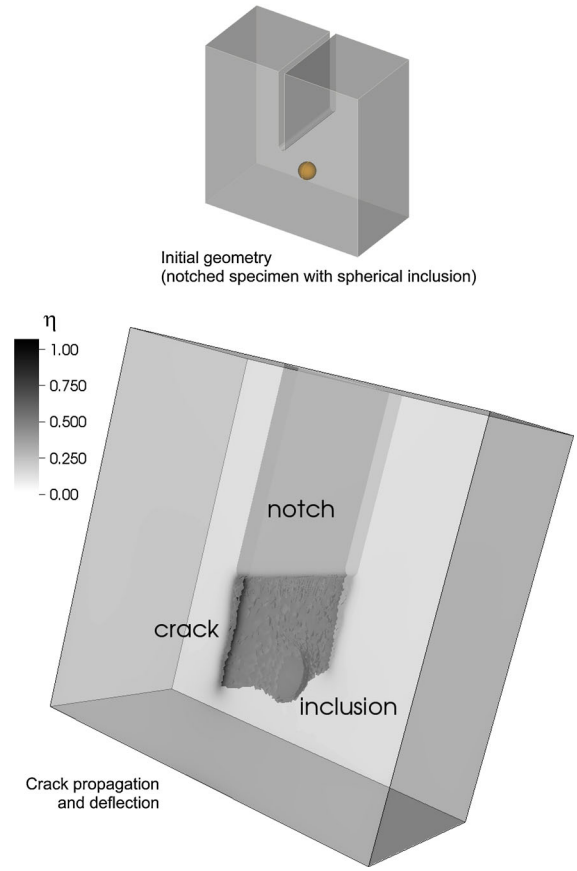

Fig. 4 Phase field prediction of crack deflection around a strong second-phase inclusion of radius $R_\mathrm{I} = 7.5l$ for far-field mode I loading ($\Gamma/\Gamma_0 = 5, \lambda/\lambda_0 = 1$) with failed material ($\eta > 0.7$) removed to visualize crack propagation

Numerous simulations of this inclusion–crack interaction problem are performed, wherein elastic stiffness λ and fracture energy Γ of the inclusion are varied, with analogous properties $\lambda_0 = \mu_0$ and Γ_0 of the matrix held fixed, and with the same far-field mode I boundary conditions imposed in each case. Results enable quantification of effects of properties on propagation behavior (i.e., deflection/bridging versus particle frac-

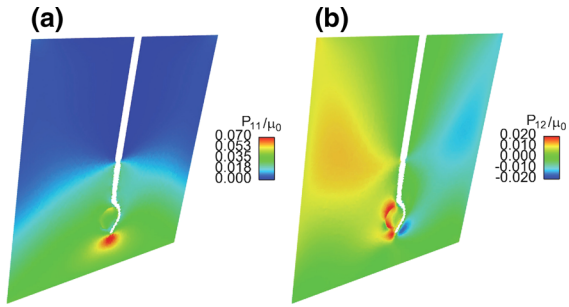

Fig. 5 Phase field predictions for stresses along mid-plane $X_3 = 0$ for crack deflection around a strong and stiff second-phase inclusion ($R_I/l = \Gamma/\Gamma_0 = \lambda/\lambda_0 = 5$) with failed material ($\eta > 0.7$) removed to visualize crack propagation: **a** normal stress component $P_{11}/\mu_0 = P_{xX}/\mu_0$ **b** shear stress component $P_{12}/\mu_0 = P_{xY}/\mu_0$ [referred here to global coordinates with (X, Y) oriented (normal, parallel) to the initial crack face]

ture) shown in Fig. 7 for $R_I = 5l$. Such trends were also found to be nearly identical for a larger inclusion with $R_I = 7.5l$ (not shown). The tendency for crack deflection to become more favorable as Γ/Γ_0 increases is understandable since surface energy increases linearly with this ratio for a planar crack splitting the inclusion. Regarding the effect of λ/λ_0, phase field predictions in Fig. 7 agree with trends derived analytically via linear elastic fracture mechanics (He and Hutchinson 1989) for penetration or deflection of a straight crack by a planar interface separating two isotropic linear elastic materials: deflection becomes more favorable as the modulus of the potentially penetrated material increases.

5 Conclusions

A new phase field theory of fracture has been implemented in 3D simulations, with results validated for isotropic and anisotropic cracking in a homogeneous material under distinct mode I and mode II far-field loading conditions. Potential crack deflection around a second-phase inclusion has been studied, demostrating effects of relative stiffness and strength of the inclusion to that of the surrounding matrix material. These results are thought profound with regards to the possible design of tailored nanocomposites with increased macroscopic toughness associated with crack bridging: second-phase particles should be selected with the appropriate properties to induce deflection, noting that a trade-off usually exists between stiffness and toughness of candidate particulate materials (e.g., stiff but weak ceramic inclusions versus compliant yet tough polymer inclusions). In other words, the present study of crack penetration versus deflection through inclusions illustrates how the phase field method might be applied to gain understanding of how nano-composites may be tailored for improved overall toughness. Future work shall consider additional geometries and property sets, the latter allowing for interfacial decohesion (Evans 1974; Xu and Needleman 1993) and cleavage anisotropy (Schultz et al. 1994), both of which can be accommodated by the present theory.

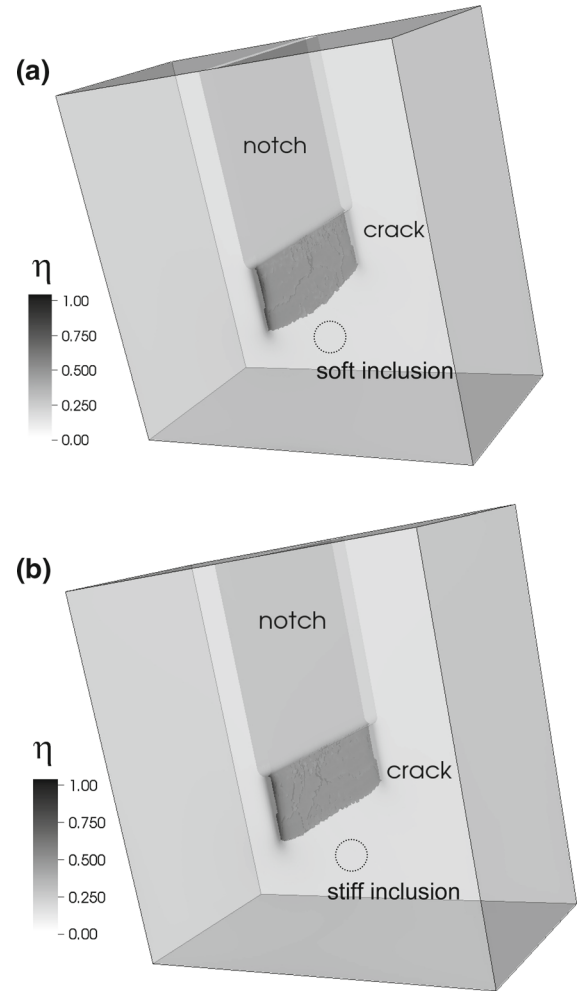

Fig. 6 Phase field prediction of crack attraction **a** towards soft ($\lambda/\lambda_0 = 0.5$) second-phase inclusion and shielding **b** by stiff ($\lambda/\lambda_0 = 10$) second-phase inclusion. In each case, the same far-field mode I boundary conditions are applied, $R_I = 5l$, $\Gamma/\Gamma_0 = 1$, and failed material ($\eta > 0.7$) is removed to visualize crack propagation

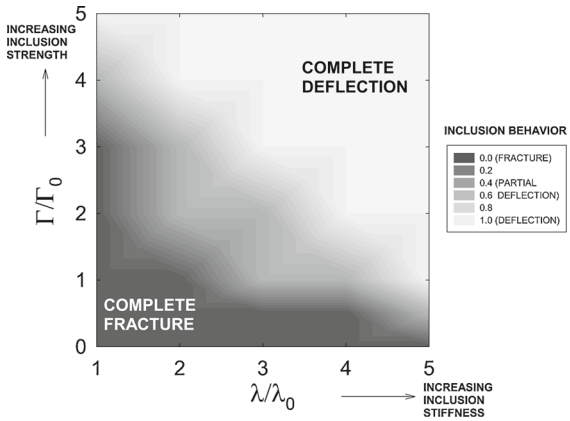

Fig. 7 Predicted tendency for mode I crack to penetrate (contour value 0) versus deflect (contour value 1) around spherical inclusion (radius $R_I = 5l$) with fracture energy Γ and initial stiffness λ, where Γ_0 and λ_0 are corresponding fixed properties of the matrix. Partial deflection is denoted by contour values between 0 and 1

The phase field method is not restricted to simple geometries and elastic linearity typical of known analytical solutions; crack propagation is insensitive to mesh construction; and no spurious parameters controlling crack propagation direction or opening displacement are required. Since ceramic crystals of interest such as alumina and silicon carbide exhibit competition among fracture, twinning, and glide of partial dislocations (Clayton 2009, 2010), future work will address such mechanisms simultaneously by assigning multiple order parameters, effectively merging the present theory with that in Clayton and Knap (2011a).

References

Abdollahi A, Arias I (2012) Numerical simulation of intergranular and transgranular crack propagation in ferroelectric polycrystals. Int J Fract 174:3–15

Alber HD (2012) A model for brittle fracture based on the hybrid phase field model. Contin Mech Thermodyn 24:391–402

Amor H, Marigo JJ, Maurini C (2009) Regularized formulation of the variational brittle fracture with unilateral contact: numerical experiments. J Mech Phys Solids 57:1209–1229

Arias I, Knap J, Chalivendra V, Hong S, Ortiz M, Rosakis A (2007) Numerical modelling and experimental validation of dynamic fracture events along weak planes. Comput Methods Appl Mech Eng 196:3833–3840

Atkinson C (1972) The interaction between a crack and an inclusion. Int J Eng Sci 10:127–136

Borden M, Verhoosel C, Scott M, Hughes T, Landis C (2012) A phase-field description of dynamic brittle fracture. Comput Methods Appl Mech Eng 217:77–95

Clayton J (2005) Dynamic plasticity and fracture in high density polycrystals: constitutive modeling and numerical simulation. J Mech Phys Solids 53:261–301

Clayton J (2006) Continuum multiscale modeling of finite deformation plasticity and anisotropic damage in polycrystals. Theoret Appl Fract Mech 45:163–185

Clayton J (2008) A model for deformation and fragmentation in crushable brittle solids. Int J Impact Eng 35:269–289

Clayton J (2009) A continuum description of nonlinear elasticity, slip and twinning, with application to sapphire. Proc R Soc Lond A 465:307–334

Clayton J (2010) Deformation, fracture, and fragmentation in brittle geologic solids. Int J Fract 163:151–172

Clayton J (2010) Modeling nonlinear electromechanical behavior of shocked silicon carbide. J Appl Phys 107:013,520

Clayton J (2011) Nonlinear Mechanics of Crystals. Springer, Dordrecht

Clayton J (2014) Finite strain analysis of shock compression of brittle solids applied to titanium diboride. Int J Impact Eng 73:56–65

Clayton J, Knap J (2011) A phase field model of deformation twinning: nonlinear theory and numerical simulation. Physica D 240:841–858

Clayton J, Knap J (2011) Phase field modeling of twinning in indentation of transparent crystals. Model Simul Mater Sci Eng 19:085,005

Clayton J, Knap J (2013) Phase-field analysis of fracture-induced twinning in single crystals. Acta Mater 61:5341–5353

Clayton J, McDowell D (2003) Finite polycrystalline elastoplasticity and damage: multiscale kinematics. Int J Solids Struct 40:5669–5688

Clayton J, McDowell D (2004) Homogenized finite elastoplasticity and damage: theory and computations. Mech Mater 36:799–824

Del Piero G, Lancioni G, March R (2007) A variational model for fracture mechanics: numerical experiments. J Mech Phys Solids 55:2513–2537

Eastgate L, Sethna J, Rauscher M, Cretegny T (2002) Fracture in mode I using a conserved phase-field model. Phys Rev E 65:036,117

Erdogan F, Gupta G, Ratwani M (1974) Interaction between a circular inclusion and an arbitrarily oriented crack. J Appl Mech 41:1007–1013

Espinosa H, Zavattieri P (2003) A grain level model for the study of failure initiation and evolution in polycrystalline brittle materials. Part I: theory and numerical implementation. Mech Mater 35:333–364

Evans A (1974) The role of inclusions in the fracture of ceramic materials. J Mater Sci 9:1145–1152

Faber K, Evans A (1983) Intergranular crack-deflection toughening in silicon carbide. J Am Ceram Soc 66:C94–C96

Foulk J, Vogler T (2010) A grain-scale study of spall in brittle materials. Int J Fract 163:225–242

Gell M, Smith E (1967) The propagation of cracks through grain boundaries in polycrystalline 3% silicon–iron. Acta Metal 15:253–258

Gilman J (1960) Direct measurements of the surface energies of crystals. J Appl Phys 31:2208–2218

Gilman J (2003) Electronic basis of the strength of materials. Cambridge University Press, Cambridge

Hakim V, Karma A (2009) Laws of crack motion and phase-field models of fracture. J Mech Phys Solids 57:342–368

He MY, Hutchinson J (1989) Crack deflection at an interface between dissimilar elastic materials. Int J Solids Struct 25:1053–1067

Hofacker M, Miehe C (2012) Continuum phase field modeling of dynamic fracture: variational principles and staggered FE implementation. Int J Fract 178:113–129

Jin Y, Wang Y, Khachaturyan A (2001) Three-dimensional phase field microelasticity theory and modeling of multiple cracks and voids. Appl Phys Lett 79:3071–3073

Kim BY, Wakayama S, Kawahara M (1996) Characterization of 2-dimensional crack propagation behavior by simulation and analysis. Int J Fract 75:247–259

Knap J, Ortiz M (2003) Effect of indenter-radius size on Au(001) nanoindentation. Phys Rev Lett 90:226,102

Knap J, Sieradzki K (1999) Crack tip dislocation nucleation in FCC solids. Phys Rev Lett 82:1700–1703

Kuhn C, Muller R (2010) A continuum phase field model for fracture. Eng Fract Mech 77:3625–3634

Lawn B (1968) Hertzian fracture in single crystals with the diamond structure. J Appl Phys 39:4828–4836

Lawn B, Padture N, Cai H, Guiberteau F (1994) Making ceramics "ductile". Science 263:1114–1116

Miehe C, Welschinger F, Hofacker M (2010) Thermodynamically consistent phase-field model of fracture: variational principles and multi-field FE implementations. Int J Numer Methods Eng 83:1273–1311

Moes N, Dolbow J, Belytschko T (1999) A finite element method for crack growth without remeshing. Int J Numer Methods Eng 46:131–150

Murrell S (1965) The effect of triaxial stress systems on the strength of rocks at atmospheric temperatures. Geophys J R Astr Soc 10:231–281

Nuismer R (1975) An energy release rate criterion for mixed mode fracture. Int J Fract 11:245–250

Ohji T, Jeong YK, Choa YH, Niihara K (1998) Strengthening and toughening mechanisms of ceramic nanocomposites. J Am Ceram Soc 81:1453–1460

Rice J (1968) Mathematical analysis in the mechanics of fracture. In: Liebowitz H (ed) Fracture: an advanced treatise. Academic Press, New York, pp 191–311

Schultz R, Jensen M, Bradt R (1994) Single crystal cleavage of brittle materials. Int J Fract 65:291–312

Spatschek R, Brener E, Karma A (2011) Phase field modeling of crack propagation. Philos Mag 91:75–95

Sun X, Khaleel M (2004) Modeling of glass fracture damage using continuum damage mechanics-static spherical indentation. Int J Damage Mech 13:263–285

Tamate O (1968) The effect of a circular inclusion on the stresses around a line crack in a sheet under tension. Int J Fract Mech 4:257–266

Voyiadjis G, Mozaffari N (2013) Nonlocal damage model using the phase field method: theory and applications. Int J Solids Struct 50:3136–3151

Wiederhorn S (1984) Brittle fracture and toughening mechanisms in ceramics. Ann Rev Mater Sci 14:373–403

Wilshaw T (1971) The Hertzian fracture test. J Phys D Appl Phys 4:1567–1581

Xu L, Huang Y, Rosakis A (2003) Dynamic crack deflection and penetration at interfaces in homogeneous materials: experimental studies and model predictions. J Mech Phys Solids 51:461–486

Xu XP, Needleman A (1993) Void nucleation by inclusion debonding in a crystal matrix. Model Simul Mater Sci Eng 1:111–132

Zhang S, Zhu T, Belytschko T (2007) Atomistic and multiscale analyses of brittle fracture in crystal lattices. Phys Rev B 76:094,114

1 (PDF) DEFENSE TECHNICAL INFORMATION CTR DTIC OCA

2 (PDF) DIRECTOR US ARMY RESEARCH LAB RDRL CIO LL IMAL HRA MAIL & RECORDS MGMT

1 (PDF) GOVT PRINTG OFC A MALHOTRA

37 (PDF) DIR USARL
RDRL CIH C
J KNAP
RDRL WM
B FORCH
J MCCAULEY
RDRL WML B
I BATYREV
B RICE
D TAYLOR
N WEINGARTEN
RDRL WML H
C MEYER
B SCHUSTER
RDRL WMM
J BEATTY
RDRL WMM B
G GAZONAS
D HOPKINS
B POWERS
C RANDOW
T SANO
RDRL WMM E
J SWAB
RDRL WMM F
M TSCHOPP
RDRL WMM G
J ANDZELM
RDRL WMP
S SCHOENFELD
RDRL WMP B
C HOPPEL
S SATAPATHY
M SCHEIDLER
A SOKOLOW
T WEERASOORIYA
RDRL WMP C
R BECKER
S BILYK
T BJERKE
D CASEM
J CLAYTON
D DANDEKAR
M GREENFIELD
R LEAVY
J LLOYD
S SEGLETES
A TONGE
C WILLIAMS
RDRL WMP D
R DONEY

INTENTIONALLY LEFT BLANK.